frontiers | Frontiers in Earth Science

TYPE Original Research
PUBLISHED 23 May 2025
DOI 10.3389/feart.2025.1585240

OPEN ACCESS

EDITED BY
Omid Haeri-Ardakani,
Department of Natural Resources, Canada

REVIEWED BY
Cun Zhang,
Qilu University of Technology, China
Mastaneh Liseroudi,
Department of Natural Resources, Canada

*CORRESPONDENCE
Muhammad Saleem Mughal,
saleem.mughal@ajku.edu.pk
George Kontakiotis,
gkontak@geol.uoa.gr

RECEIVED 28 February 2025
ACCEPTED 06 May 2025
PUBLISHED 23 May 2025

CITATION
Majeed KU, Mughal MS, Kontakiotis G, Ali SK, Akhtar S, Janjuhah HT, Siddique K, Besiou E and Antonarakou A (2025) Petrography and geochemistry of Late Carboniferous dolostone-hosted soapstone in the Sherwan Formation, Hazara Basin: insights into hydrothermal and dynamic metamorphic processes.
Front. Earth Sci. 13:1585240.
doi: 10.3389/feart.2025.1585240

Petrography and geochemistry of Late Carboniferous dolostone-hosted soapstone in the Sherwan Formation, Hazara Basin: insights into hydrothermal and dynamic metamorphic processes

Khawaja Umair Majeed[1,2], Muhammad Saleem Mughal[1]*, George Kontakiotis[3]*, Syed Kamran Ali[1], Shamim Akhtar[4], Hammad Tariq Janjuhah[5], Kamaran Siddique[1], Evangelia Besiou[3] and Assimina Antonarakou[3]

[1]Institute of Geology, University of Azad Jammu and Kashmir, Muzaffarabad, Pakistan, [2]School of Geological Engineering and Surveying, Chang'an University, Xi'an, China, [3]Department of Historical Geology and Paleontology, Faculty of Geology and Geoenvironment, National and Kapodistrian University of Athens, Athens, Greece, [4]Department of Earth Sciences, University of Sargodha, Sargodha, Pakistan, [5]INTI, International University Nilai, Negeri Sembilan, Malaysia

Introduction: This study investigates the petrography and geochemistry of soapstone-bearing dolomite within the Sherwan Formation, Hazara Basin, with a focus on understanding hydrothermal dynamic metamorphism and resolving the age controversy surrounding the host rock.

Methods: Field observations, petrographic analysis, and geochemical techniques were used, including X-ray diffraction (XRD), scanning electron microscopy (SEM), and energy-dispersive spectroscopy (EDS), to characterize mineral composition and alteration processes.

Results: Petrographic evidence confirms that talc formed through hydrothermal alteration of Late Carboniferous dolomite, facilitated by faulting, folding, and silica-rich fluid infiltration. Distinct geological features such as stromatolitic dolomite, pseudotachylitic veins, and mylonitization suggest episodic brittle deformation under high-temperature conditions. The presence of *Anthracoporella spectabilis* supports a Late Carboniferous age for the dolomite, while the soapstone is dated to the Permian, linked to Pre-Himalayan tectonics, Panjal volcanism, and dolerite intrusions. Mineralogical analyses reveal that soapstone is primarily composed of talc (steatite), with secondary minerals including brucite, magnesite, willemseite, and montmorillonite. The occurrence of pyrite and hematite indicates hydrothermal interactions, contributing to metal enrichment and oxidation.

Discussion: Geochemical data show silica enrichment and structural weakening as key factors in dolomite-to-talc transformation. Trace levels of chromium (100–300 ppm) raise concerns over Cr^{6+} toxicity, but the absence of arsenic,

lead, cadmium, and mercury supports the environmental safety and industrial potential of the soapstone. The study underscores the complex interplay of tectonic, metamorphic, and geochemical processes in the evolution of the Sherwan soapstone.

KEYWORDS

Permian soapstone-bearing dolomite, hydrothermal metamorphism, Late Carboniferous dolomite, Pre-Himalayan orogeny, geochemical analysis, fluid-rock interactions

1 Introduction

Talc is a hydrous magnesium silicate that forms predominantly through metasomatic and metamorphic processes and is typically hosted in magnesium carbonate rocks and ultramafic bodies (Anderson et al., 1990; Hecht et al., 1999; Zedef et al., 2000). Globally, talc deposits are classified into three main genetic types, magmatic hydrothermal often associated with mafic-ultramafic intrusion, regional metamorphic related to greenschist to amphibolite facies conditions and sedimentary diagenetic where talc replaces dolomite in shallow basinal environments (Groppo and Compagnoni, 2007; Prochaska, 1989; Woelfler et al., 2015). Each type varies based on fluid composition, protolith mineralogy, pressure-temperature (P-T) conditions and the structural framework (Schandl et al., 2002; Moine et al., 1989).

Talc commonly develops along fault zones or shear bands where structural permeability facilitates the influx of MgO and SiO_2 rich fluids under moderate temperature and pressure typically within greenschist facies conditions (Barbosa and Castillo, 2023; Shin and Lee, 2003). Its formation is influenced by decarbonation reaction especially in carbonate rich rocks like dolomite and fluid rock interactions that drive mineralogical transformations. However, the presence of Al, Ca and K in the protolith can hinder talc stability and promote competing hydrous silicates such as chlorite, phlogopite or tremolite (Bucher and Grapes, 2011). The role of plate tectonics is crucial in this process, as it promotes fluid infiltration and subsequent mineralogical changes (Easthouse et al., 2025; Pudsey et al., 1985).

Several studies have described talc formation in diverse geological settings including the Eastern Alps, Western Canada and central Turkey providing analogues for dolomite hosted talc deposits formed via hydrothermal dynamic metamorphism (Blount and Vassiliou, 1980; Evans and Guggenheim, 1988). However, the Sherwan Formation in the Hazara Basin of northern Pakistan remains less well understood, especially regarding the timing and mechanism of talc mineralization. The region has undergone multiple tectono-thermal events related to Pre-Himalayan and Himalayan orogeny's which likely influenced by fluid migration and mineral alteration (Joshi and Sharma, 2015; Sajid et al., 2018).

This study investigates the petrographic and geochemical characteristics of dolomite hosted soapstone within the Sherwan Formation, Hazara Basin aiming to understand the role of hydrothermal dynamic metamorphism in talc genesis. Though an integrated approach combining field observation, petrographic analysis and geochemical data, the study identifies mineral assemblages, textures and chemical trends associated with talc formation. Analytical techniques include XRD, SEM for mineral characterization and bulk chemical analysis for compositional data. The results help constrain the metamorphic conditions and fluid interactions responsible for talc formation while also contributing to the ongoing discussion on the age and evolution of the Sherwan Formation, Hazara Basin. Additionally, the study addressed the longstanding controversy surrounding the age of Sherwan Formation, Hazara Basin by examining lithological characteristics and alteration patterns. The findings contribute to a broader understanding of talc deposits genesis particularly dolomite-hosted types and the role of hydrothermal processes in shaping Earth's mineral resources (Prochaska, 1989).

1.1 Study area

Large deposits of soapstone are exposed in the Sherwan area of Abbottabad, Hazara. Several mines in this area are mining premium quality of soapstone for industrial applications. This study examined the dolomite of the Sherwan Formation in the Khandakhu Mine, located 42 km from Abbottabad. The Khandakhu mine is located in the geographical coordinates 34° 10′11.05″N and 73° 02′49.2″E.

1.2 Geological and tectonic setting

The Hazara Basin, located in the northwestern Himalayan orogenic belt of Pakistan, forms part of the NE-SW trending Lesser Himalayan tectonostratigraphic zone. It contains a thick sedimentary succession ranging from Precambrian to Miocene, including alternating clastic and carbonate sequences that record the complex depositional and tectonic history of the region (Ahsan and Chaudhry, 1998; Chaudhry et al., 1997; Fazal et al., 2022; Zaheer et al., 2022; Rehman et al., 2023). The basin's evolution reflects polyphase deformation linked to the convergence and eventual collision of the Indian and Eurasian plates. During the Late Cretaceous (~100 Ma), the Kohistan-Ladakh Island Arc (KIA) collided with the Eurasian Plate along the Shyok Suture Zone, initiating a major tectonic event in northern Pakistan (Pudsey et al., 1985; Treloar et al., 1989). This was followed by the obduction of the KIA onto the Indian Plate between ~85 and 50 Ma along the Main Mantle Thrust (MMT), the western extension of the Indus-Tsangpo Suture, resulting in crustal shortening, accretion, and significant structural complexity (Kazmi and Jan, 1997; Le Fort, 1975). The subsequent India-Asia continental collision during the Early Eocene (~55–50 Ma) triggered widespread deformation across the Himalayan belt. In the Hazara Basin, this is reflected in major structural features such as the Panjal Thrust, Maira Anticline, and Darband Fault, which define the southern, eastern, and western

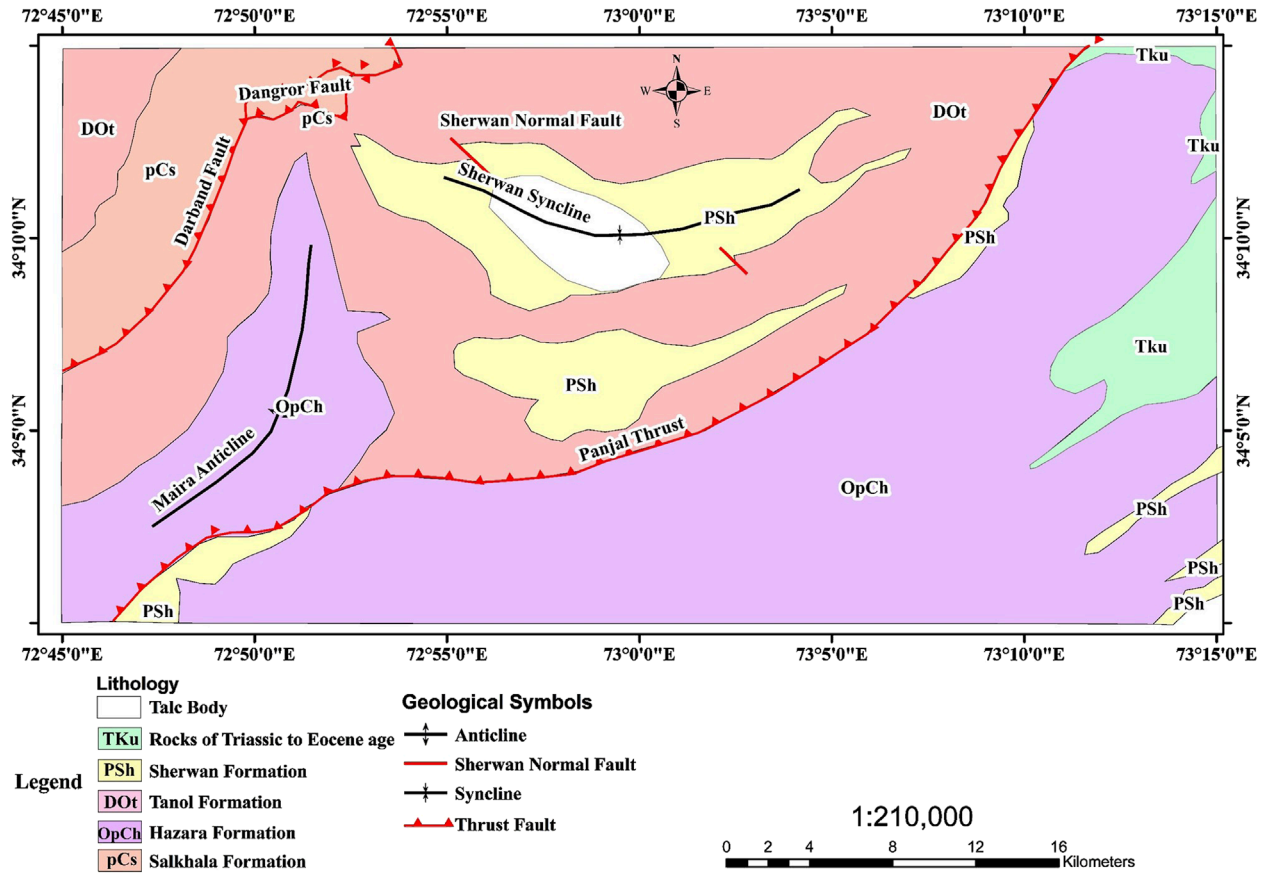

FIGURE 1
Geological map of the study area modified after (Calkins et al., 1975).

boundaries of the study area (Figure 1). These structures record a complex interplay of compressional and extensional forces, and their associated faults, folds, and synclines have played a key role in controlling fluid flow and deformation pathways critical factors in the formation and localization of talc mineralization.

Magmatic activity associated with the Kohistan Arc (Jurassic to Eocene) and post-collisional intrusions influenced regional geothermal gradients. Although major plutons are absent in the immediate study area, the thermal impact of nearby arc-related magmatism is believed to have facilitated regional metamorphism and fluid mobilization (Petterson and Windley, 1985; Treloar et al., 1989). During the Oligocene to Miocene, the basin experienced greenschist-facies metamorphism, under which dolostone units in the Sherwan Formation were altered to talc-bearing soapstone. This alteration occurred primarily through dynamic metasomatism along structurally prepared zones such as shear bands and thrusts (Bucher et al., 2002; Shin and Lee, 2003). Petrographic evidence, including porphyroblastic talc, brucite, pseudotachylitic textures, and mylonites, indicates multistage deformation and recrystallization. Since the post-Miocene, the area has undergone significant uplift, exhumation, and erosion, which has exposed soapstone bodies at the surface. These processes also led to oxidative weathering and trace element redistribution, as evidenced by the presence of environmentally sensitive elements such as chromium and sulfur in the altered rocks. These elements serve as proxies for understanding past environmental conditions, with their concentrations reflecting changes in weathering and oxidation states (Konhauser et al., 2011; Carroll, 1970). The formation of talc in the Sherwan area is thus interpreted as the product of a tectonically driven hydrothermal metamorphic system, consistent with dolomite-hosted talc deposits described in other orogenic belts, such as the Eastern Alps and central Anatolia (Prochaska, 1989; Groppo and Compagnoni, 2007). The integration of field relationships, petrographic textures, and geochemical signatures with the documented regional tectonomagmatic framework supports a robust paragenetic model for talc genesis in the Hazara Basin. The study area contains synclinal structures, characterized by the presence of dolomite in the core and the Tanol Formation in the limbs. The formation of the Sherwan normal fault can be attributed to the development of extensional forces within the core of the syncline. Notably, the dolomite in the fracture zone of the Sherwan normal fault had undergoes a transformation into talc.

2 Methodology

A detailed fieldwork was conducted in the study area, where fresh samples were collected from the Hazara Basin formation. All collected rock samples were cut and ground in the laboratory to make

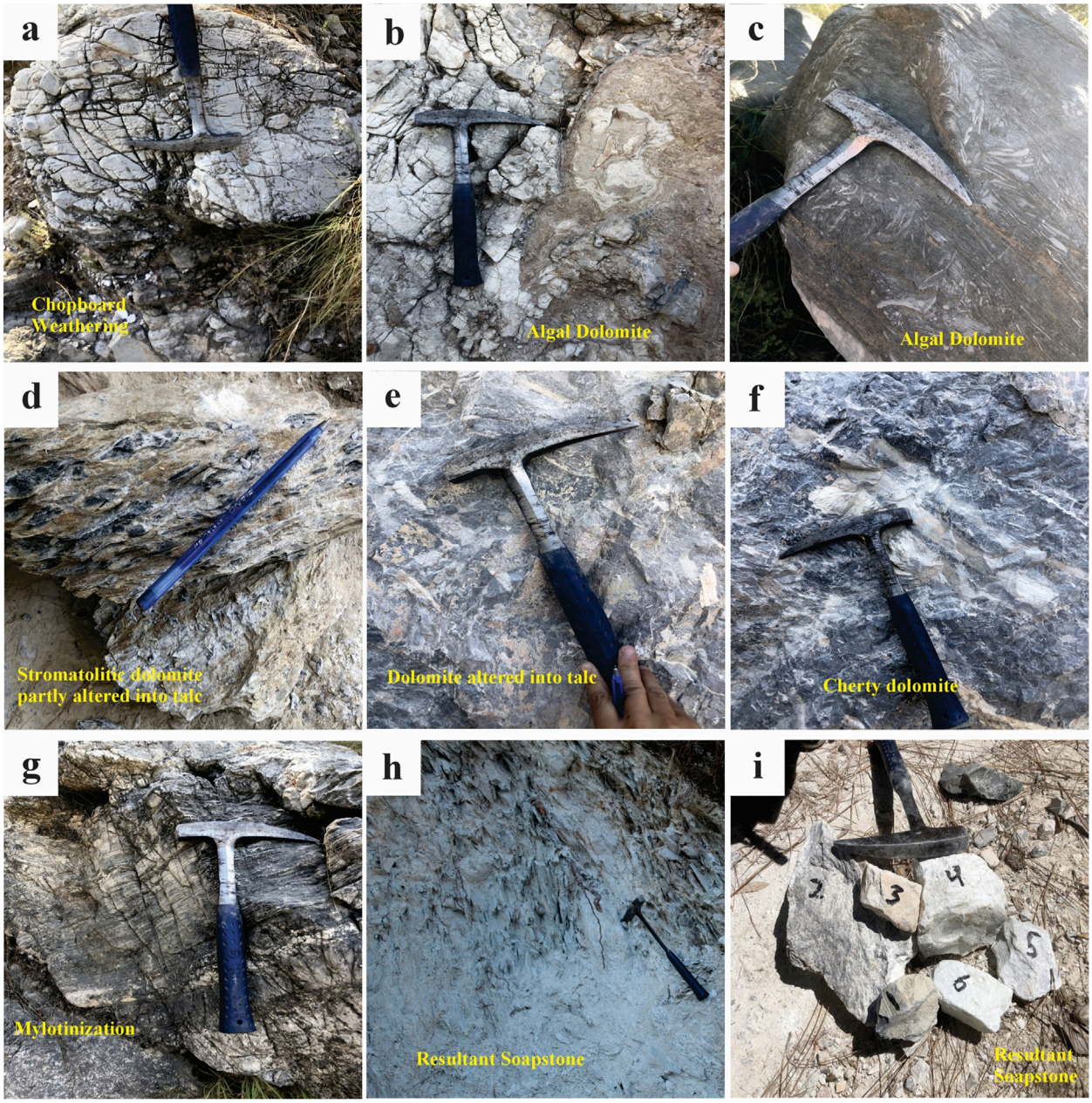

FIGURE 2
Field photographs showing soapstone formation and associated geological features in the Sherwan area, **(a)** chopboard weathering patterns on dolomite, highlighting structural weaknesses and initial weathering, **(b,c)** algal dolomite (Anthracoporella spectabilis) with stromatolithic textures, suggesting a biochemical origin and precursor lithology, **(d)** stromatolithic dolomite partially altered into talc, demonstrating hydrothermal fluid infiltration, **(e)** dolomite altered into talc through hydrothermal metamorphism, **(f)** cherty dolomite enriched with siliceous material, associated with metasomatic processes, **(g)** evidence of mylonitization in dolomitic rocks, indicating intense shearing and tectonic deformation, **(h)** *in situ* soapstone outcrop, representing the final product of dolomite alteration, **(i)** collected soapstone samples for geochemical and petrographic analysis, showing variable textures and mineralogy.

thin sections for petrographic studies. A detailed examination was carried using a polarizing microscope. Following the petrographic analysis, most of the samples collected were grounded and made into powder pallets for additional laboratory analyses, including X-ray diffraction (XRD), X-ray fluorescence (XRF), and scanning electron microscopy (SEM), to gain a better understanding of their mineralogical composition and correlate these findings with the geological history and tectonic evaluation of the Hazara Basin.

The SEM images and XRD analyses were performed at the Centralized Resource Laboratory, University of Peshawar, Pakistan, while the XRF analysis was performed at the Chinar group of companies in Islamabad and School of Geological Engineering and Surveying, Chang'an University. X-ray diffraction patterns were obtained for mineral identification using the 'Jade' software, at the Institute of Geology, University of Azad Jammu and Kashmir, Muzaffarabad, Pakistan.

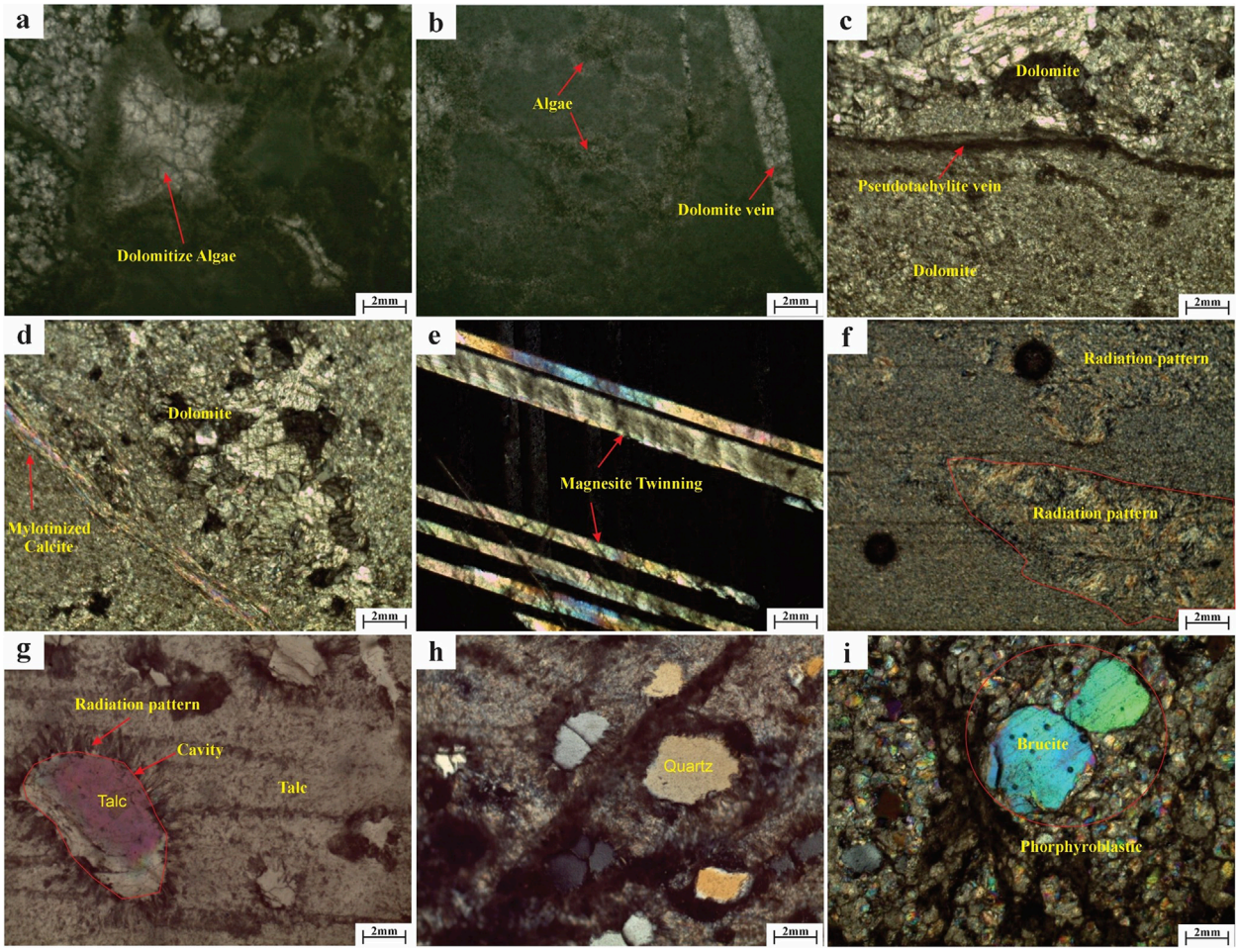

FIGURE 3
Petrographic analysis of the samples showing various textures and mineralogical features: **(a)** dolomitized algae (*Anthracoporella spectabilis*), indicating microbial activity and diagenetic alteration, **(b)** dolomite vein cutting through algal structures, suggesting fluid infiltration and mineralization, **(c)** pseudotachylite vein within dolomite, representing brittle deformation and localized melting, **(d)** mylonitized calcite within dolomite, highlighting ductile deformation under high strain, **(e)** magnesite twinning, indicative of deformation and recrystallization, **(f)** radiation pattern in mineral grains, possibly formed due to nucleation and radial growth, **(g)** talc mineral with a cavity and radiation pattern, suggesting hydrothermal alteration, **(h)** quartz grain within the matrix, indicating detrital or metamorphic origin, **(i)** brucite shows porphyroblastic texture with distinct birefringence, representing metamorphic overgrowth and recrystallization.

Rock powders were prepared for SEM analysis using the 'JSM-IT100' scanning electron microscope at the NCEG, University of Peshawar, Pakistan. The cut samples were attached to a SEM specimen plug with double carbon tape and coated with conductive metal gold (Au) in an evaporative coater. The coated samples were placed in the electron optics column of the sample chamber, which was evacuated to a high vacuum.

3 Results

3.1 Field study

In Sherwan area, talc mineralization occurs predominantly within dolomitic rocks exposed along fault and shear zone. The dolomite displays chopboard weathering patterns (Figure 2a). Algal structures identified as Anthracoporella spectabilis, are preserved in dolomite with stromatolitic texture (Figures 2b,c). Chert dolomite is also observed (Figure 2d). In several locations dolomite transform into talc while preserving boudinage textures (Figure 2e). Structural deformation features include mylotinization and brittle fracturing (Figures 2f,g). Soapstone is observed *in situ* at several locations (Figure 2h) and samples were collected for analysis (Figure 2i).

3.2 Petrography

Petrographic analysis shows that soapstone primarily consists of talc (steatite) with associated minerals including quartz, brucite, magnesite, pyrite, hematite and lazurite. Dolomite exhibits planar and non-planar textures with evidence of replacement of earlier calcite veins (Figures 3a,b). Pseudotachylite veins cut across dolomite in deformed zones (Figure 3c) and calcite shows ductile deformation features while dolomite displays brittle fracturing (Figure 3d). Rainbow twinning is observed in magnesite grains

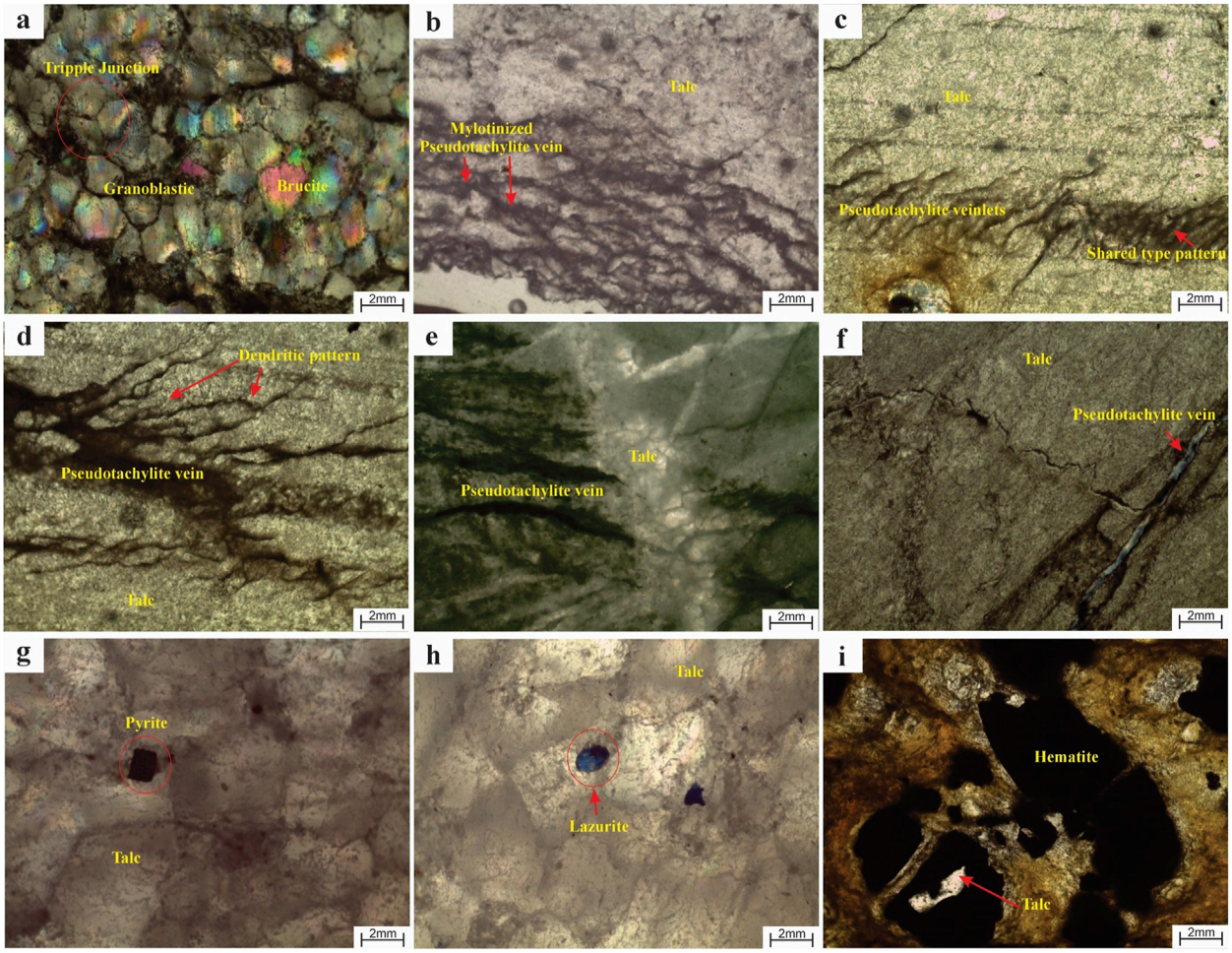

FIGURE 4
Petrographic analysis of the sample showing various textures and mineralogical features: **(a)** brucite shows granoblastic texture with equigranular grains and triple junctions indicating recrystallization under static metamorphic conditions, **(b)** mylonitized pseudotachylite vein within talc, suggesting ductile deformation followed by brittle failure and melting, **(c)** pseudotachylite veinlets in talc with a shared-type pattern, indicative of hydrothermal activity and mechanical deformation, **(d)** dendritic pattern within a pseudotachylite vein, formed due to rapid crystallization under high strain and rapid cooling, **(e)** pseudotachylite vein surrounded by talc, representing brittle failure followed by talc alteration during retrograde metamorphism, **(f)** pseudotachylite vein in talc, highlighting repeated brittle deformation events and rapid quenching, **(g)** pyrite crystal within talc, formed through sulfur-rich hydrothermal fluid interactions under reducing conditions, **(h)** lazurite grains in talc, suggesting multiple metamorphic events, **(i)** hematite replacing talc indicate oxidation processes.

(Figure 3e). Talc commonly exhibits radiating crystal habits and porphyroblastic textures (Figures 3f, g, i). Quartz grains are scattered within the soapstone matrix (Figure 3h).

Brucite also forms large porphyroblasts. Granoblastic textures with 120° triple junction are seen in brucite (Figure 4a). Pseudotachylite veins within talc show sheared margins, dendritic structures and mylonitic overprints (Figures 4b–f). Pyrite (up to 3%) occurs as cubic grains (Figure 4g) and lazurite is present in discrete grains (Figure 4h). Hematite partially replaces talc in some samples (Figure 4i).

3.3 Xray diffraction (XRD)

The XRD analysis confirms the mineralogical composition identified in the petrographic study, with talc ($Mg_3Si_4O_{10}(OH)_2$) being the dominant phase across all samples. The patterns display sharp and well-defined peaks, indicative of the crystalline nature of the minerals (Figures 5a–c). In Figure 5a, talc exhibits the highest intensity peaks, highlighting its abundance. Minor peaks corresponding to brucite ($Mg(OH)_2$) and magnesite ($MgCO_3$) are also present, suggesting their occurrence as secondary phases. Figure 5b shows a similar mineral assemblage, with additional reflections corresponding to willemseite ($(Ni,Mg)_3Si_4O_{10}(OH)_2$) and montmorillonite ($(Na,Ca)_{0.3}(Al,Mg)_2Si_4O_{10}(OH)_2{\cdot}nH_2O$). Willemseite is identified by distinct peaks in the lower 2θ region. Talc remains the most prominent mineral phase, based on the relative intensity of its peaks.

In Figure 5c, a broader range of minerals is detected. Besides talc, strong peaks for montmorillonite indicate a significant presence. Minor peaks of willemseite and brucite are also noted, further supporting the mineral diversity in this sample. Overall, the XRD data confirm that talc is the principal mineral, while brucite,

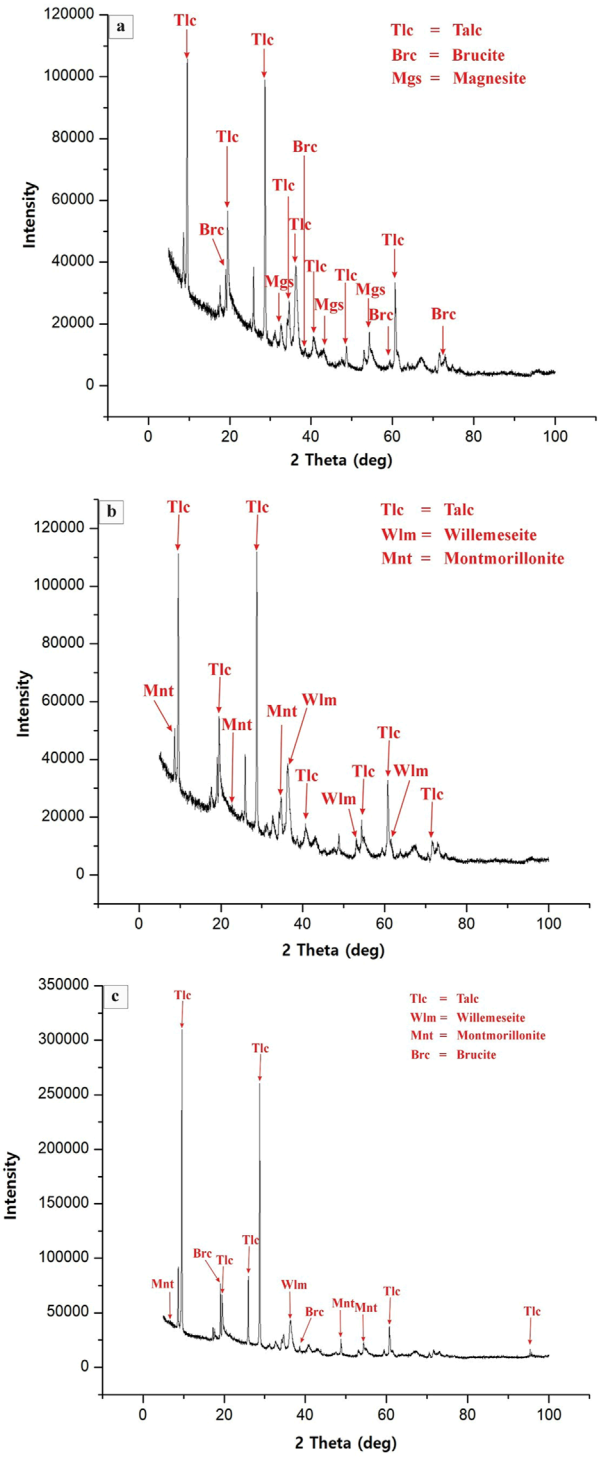

FIGURE 5
X-ray diffraction (XRD) patterns of three samples showing mineralogical compositions: **(a)** Talc (Tlc), Brucite (Brc) and Magnesite (Mgs); **(b)** Talc (Tlc), Montmorillonite (Mnt) and Willemseite (Wlm); **(c)** Talc (Tlc), Montmorillonite (Mnt) and Brucite (Brc).

magnesite, willemseite, and montmorillonite are present in varying amounts. Variations in peak intensity and 2θ position reflect their relative abundances and crystalline quality.

3.4 Scanning electron microscope (SEM)

The Scanning Electron Microscopy (SEM) images reveal the microstructural features of a mineral assemblage that includes talc, brucite, magnesite, and dolomite. These images show a complicated intergrowth of various minerals, with talc showing as thin, flaky, and platy sheets that indicate its layered silicate structure. Brucite exhibits tiny, needle like structures in aggregates, indicating its hydroxide content. Magnesite occurs as irregular grains, while dolomite is characterized by rhombohedral crystals with well-developed cleavage lines (Figures 6a,c,e).

The associated Energy Dispersive X-ray Spectroscopy (EDS) spectra validate the elemental composition, with peaks for Mg, Si, O, C, Ca, and Fe supporting the mineral identification. The presence of Fe in some spectra suggests minor iron substitution, which may influence mineral stability (Figures 6b,d,f).

3.5 Soapstone major and trace element geochemistry

The major and trace element compositions of representative soapstone samples are provided in Table 1. The chemical analysis indicates that SiO_2 content in soapstone ranges from 30.61 to 81.56 wt%. The bulk compositions of Sherwan soapstone plot along the calcite-antigorite tie-line in the CaO-MgO-SiO_2 ternary diagram, primarily due to the highly variable concentration of CaO and CO_2 and nearly constant Mg/Si ratios (Figure 7). This indicates significant carbonate metasomatism and decarbonation processes. The compositional spread underscores the influence of precursor dolomitic lithologies and hydrothermal alteration on the soapstone's chemistry. The alignment along the calcite, antigorite tie-line highlights the critical role of silica- and magnesium-rich fluids during metamorphism. These findings provide insights into the physicochemical conditions responsible for the soapstone's evolution (Figure 7). The bulk rock compositional variations of soapstone from the Sherwan area, illustrated on a CaO-MgO-SiO_2 (CMS) ternary diagram, predominantly align along the calcite–antigorite tie-line. The alignment reflects the interplay of calcite, antigorite, and minor talc, driven by variable CaO and CO_2 contents while maintaining a nearly constant Mg/Si ratio. Notably, the evaluated soapstone samples were free from measurable amounts of arsenic (As), lead (Pb), cadmium (Cd), and mercury (Hg), suggesting that these key hazardous elements are not a concern in the researched material. However, given the presence of chromium, particularly the potential for its dangerous hexavalent form in numerous samples, further study is essential to assure safety and compliance with health and environmental regulations.

4 Discussion

The petrographic, geochemical, and structural evidence from the Sherwan area supports a multi-phase geological history involving tectonic deformation, hydrothermal fluid flow, and dynamic metamorphism, which collectively facilitated the transformation of dolomite into talc-rich soapstone deposits. Field observations show that talc occurrences are localized along fault zones, shear

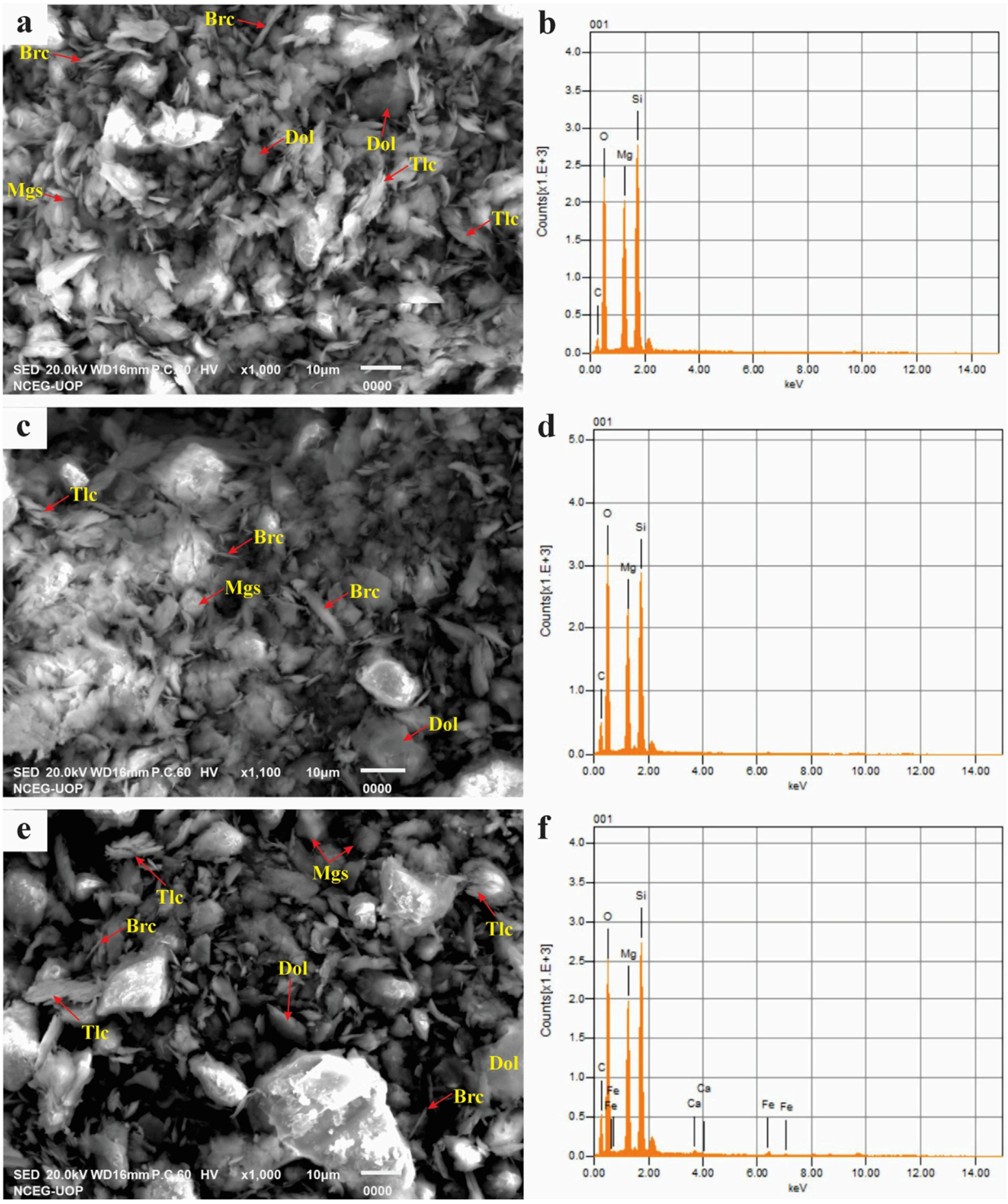

FIGURE 6
Scanning electron microscopic (SEM) and Energy Dispersive X-ray Spectroscopy (EDS) patterns of three samples showing mineralogical compositions: **(a,c,e)** shows talc (Tlc), brucite (Brc), magnesite (Mgs) and dolomite (Dol), **(b,d,f)** shows elemental composition, with peaks for Mg, Si, O, C, Ca, and Fe.

bands, and fractured dolomitic units. These structural discontinuities likely served as pathways for hydrothermal fluids during multiple deformation events. The Sherwan Formation, deposited during the Late Carboniferous, underwent significant tectonic reactivation during both the Pre-Himalayan and Himalayan orogenic events (Joshi and Sharma, 2015; Sajid et al., 2018). The presence of boudinage structures, mylonitic textures, and pseudotachylitic veins supports episodic brittle and ductile deformation under varying pressure-temperature regimes, consistent with dynamic metamorphism (Molnar and Tapponnier, 1975).

10.3389/feart.2025.1585240

TABLE 1 Major and Trace elements of Soapstone, Sherwan, Abbottabad.

Sample no.	ST1	ST2	ST3	ST4	ST5	ST6	ST7	ST8	ST9	ST10	ST11	ST12	ST13	ST14	ST15	ST16
SiO_2	57.80	53.68	63.03	36.64	68.06	63.29	61.29	68.14	59.63	67.75	61.19	81.56	65.35	30.61	63.04	62.27
Al_2O_3	0.38	1.96	—	0.22	0.28	0.57	—	—	—	—	—	0.81	—	5.45	—	—
FeO	0.34	1.63	0.27	0.79	0.31	0.93	0.31	0.66	0.26	0.46	0.50	0.19	0.89	0.69	3.15	7.98
CaO	3.62	0.42	0.15	22.99	0.38	0.27	0.27	0.15	0.66	0.21	0.22	0.27	0.15	22.48	0.69	0.38
MgO	32.38	30.66	31.77	20.14	26.70	33.00	30.50	34.55	28.94	34.60	30.72	22.33	32.75	40.08	31.72	32.21
K_2O	—	—	—	0.01	-	—	—	—	—	—	—	—	—	0.02	—	—
P_2O_5	0.05	0.18	0.02	0.14	0.16	0.07	0.02	0.05	0.23	0.02	0.05	0.05	—	0.16	0.37	0.11
Trace elements in ppm																
S	—	—	—	—	—	400	—	—	—	—	—	—	—	—	1100	5700
Cl	—	—	—	900	—	—	—	—	—	—	—	—	—	900	—	—
Ti	100	1300	—	—	—	1500	—	—	—	—	—	—	—	1000	400	100
Cr	100	200	100	200	100	100	100	100	200	200	100	200	100	300	100	100
Mn	100	—	—	400	—	—	—	—	—	—	—	—	—	400	100	—
Sr	—	—	—	100	—	—	—	—	—	—	—	—	—	100	—	—
Zr	—	200	100	—	100	300	—	100	300	—	—	—	—	100	200	100
Rh	—	—	—	—	—	—	—	—	—	100	—	—	—	—	—	—
Ba	—	—	100	—	—	—	—	—	—	—	—	—	—	—	—	—
La	—	100	—	—	—	—	—	—	—	—	—	—	—	—	—	—

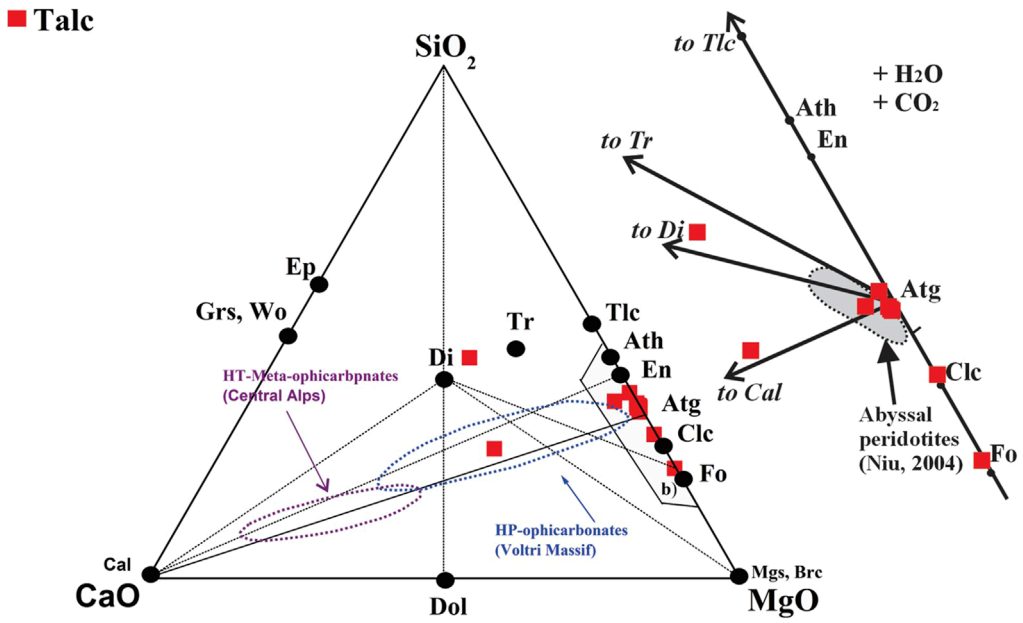

FIGURE 7
Bulk rock compositional variations of soapstone from Sherwan area, CaO-MgO-SiO_2 (CMS) ternary compositional diagram with molar whole rock proportions and projected mineral endmembers for comparison (Scambelluri et al., 2016).

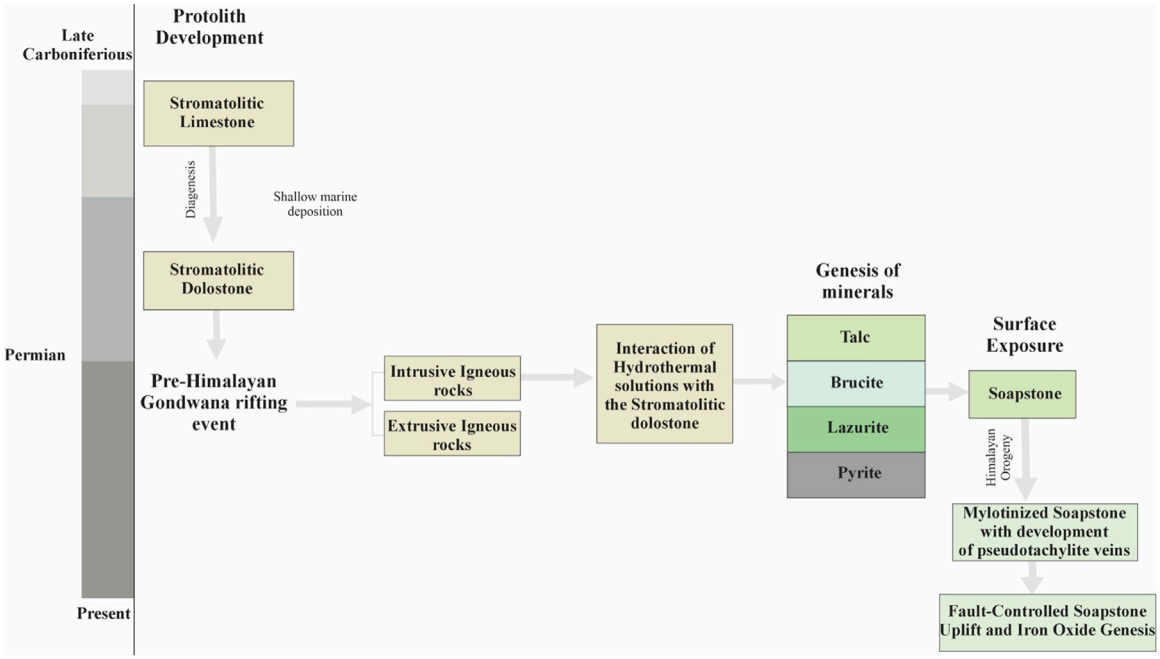

FIGURE 8
Schematic diagram illustrating the four-stage paragenetic evolution of soapstone mineralization: protolith development, pre-Himalayan hydrothermal alteration, genesis of mineral and surface exposure.

The transformation of dolomite into talc in structurally weakened zones is evidenced by the preservation of algal textures, stromatolitic layering, and chopboard weathering. These features suggest that talc alteration retained some of the primary lithological characteristics of the protolith. The co-occurrence of quartz, brucite, and magnesite with talc supports metasomatic alteration involving silica and magnesium rich hydrothermal fluids, possibly derived from deeper magmatic or sedimentary sources. This interpretation aligns with previous work indicating that quartz-saturated hydrothermal fluids can replace dolomite with talc

through fluid-rock interaction (Hecht et al., 1999; O'Hanley, 1996). Petrographic features such as porphyroblastic talc and brucite, 120° triple junctions in brucite, radiating talc textures, pseudotachylitic veins, and mylonitic shear fabrics reflect multistage metamorphism. These textural variations highlight shifts between static and dynamic recrystallization under differential stress fields. Notably, rainbow twinning in magnesite and ductile behavior in calcite contrast with brittle deformation in dolomite, indicating mineral-specific rheological responses (Molnar and Tapponnier, 1975). XRD and SEM-EDS analyses confirm the mineralogical and chemical composition of soapstone, with talc as the dominant phase and secondary minerals including brucite, magnesite, willemseite, montmorillonite, and quartz. SEM imagery shows flaky talc, fibrous brucite, irregular magnesite grains, and rhombohedral dolomite, while EDS spectra reveal Fe, Mg, Si, Ca, and minor S peaks. These features are consistent with a low-to medium-grade metamorphic overprint and metasomatic alteration in a tectonically active environment (O'Hanley, 1996).

Geochemical data show that Sherwan soapstone compositions align with the calcite–antigorite tie-line in the CaO-MgO-SiO_2 ternary diagram, suggesting carbonate metasomatism and decarbonation. This trajectory reflects silica enrichment and relative Ca removal while preserving Mg/Si ratios processes typical of talc formation in ultramafic and dolomitic settings affected by hydrothermal fluids (Scambelluri et al., 2016).

Further complexity in the metamorphic history is indicated by the occurrence of lazurite, which appears to be overprinted onto pre-existing talc. Its presence, along with late-stage hematite, suggests multiple hydrothermal and metamorphic pulses, potentially related to evolving redox conditions during retrograde metamorphism (Cuitino, 2010; Groves and Yue, 2009; Hill, 2018; McGrath, 2017; Vezzoni et al., 2020). These mineralogical transitions reflect shifts from reducing to oxidizing conditions, possibly caused by changes in fluid composition or temperature. The petrographic identification of algal textures and fossiliferous microstructures including well preserved *Anthracoporella spectabilis* confirms a Late Carboniferous age for the dolomitic protolith in the Sherwan Formation, Hazara Basin. These microfossils typically associated with shallow marine carbonate environment are widely recognized as biostratigraphic marker for upper Carboniferous strata (Groves and Yue, 2009). The stromatolithic fabric and chopboard weathering observed under the microscope further support this interpretation, reflecting low-energy, shallow water depositional setting that typify Carboniferous peritidal dolostone platform (Riding, 2000; Rowland and Shapiro, 2002). In contrast the alteration of dolomite to talc characterized by the development of talc, brucite and quartz assemblages and metasomatic textures is attributed to Permian hydrothermal activity associated with Gondwana rifting and the emplacement of Panjal volcanics and dolerite intrusion as also suggested by Sajid et al. (2018) and comparable findings from talc bearing carbonate system in Central Asia and Turkey (Prochaska, 1989; Zedef et al., 2000).

The collective data support a paragenetic model in which talc formed through a four-stage evolutionary process: (a) deposition of stromatolitic limestone in a shallow marine environment during the Late Carboniferous period, followed by diagenetic transformation into stromatolitic dolostone. This stage established the biological and sedimentary framework, including stromatolites and algal fossils (*A. spectabilis*), forming the base for talc-hosted units, (b) during the Gondwana rifting event, magmatic activity including intrusive (dolerite) and extrusive (Panjal volcanics) rocks facilitated the generation and circulation of hydrothermal solutions rich in silica and magnesium. These fluids interacted with the stromatolitic dolostone, leading to metasomatic alteration and decarbonation, forming talc, brucite, and associated mineral phases (Sajid et al., 2018), (c) genesis of mineral assemblages continued interaction and metamorphic conditions resulted in the formation of talc, brucite, lazurite, and pyrite. These mineral assemblages represent the key mineralogical expression of the altered dolostone units and (d) during the Himalayan orogeny, compressional tectonic forces reactivated preexisting structural weakness, resulting in the uplift of mylotinized soapstone, accompanied by intense recrystallization and deformation. This tectonic activity furter facilitated the formation of pseudotachylite veins and promoted oxidative alteration processes, leading to the development of iron oxides (Hematite). Late-stage metamorphism further modified the mineralogy, resulting in secondary growth of brucite, recrystallized talc, and overprints of hematite formed via oxidative weathering of pyrite. Post-orogenic uplift and erosion exposed the mineralized zones at the surface. Weathering processes altered pyrite to hematite and talc-brucite assemblages formed soapstone, now observable in outcrop. Minor structures like pseudotachylite were also preserved during this uplift phase (Figure 8).

5 Conclusion

1. This study demonstrates that the formation of soapstone in the Sherwan area resulted from the hydrothermal dynamic metamorphism of Late Carboniferous dolomite, facilitated by structurally controlled fluid flow along faults, shear bands and fractures. tectonic reactivation during both Pre-Himalayan and Himalayan orogeny's played a critical role in localizing deformation and channeling mineralization fluids as evidenced by field structures such as pseudotachylitic veins, boudinage zone, mylonite's and stromatolithic dolomite textures.
2. Petrographic, mineralogical and microstructural analysis including thin section, XRD, SEM and EDS confirms that the soapstone is composed predominantly of talc (steatite) with accessory brucite, magnesite, quartz, willemseite and montmorillonite. The occurrence of porphyroblastic talc, 120° triple junction in brucite and rainbow twinning in magnesite indicates metamorphic recrystallization under variable pressure temperature regimes. The presence of lazurite and hematite overprinting earlier talc assemblages suggest multiphase hydrothermal and retrograde metamorphic events.
3. Geochemical data support a metasomatic origin for talc, with sample composition trending along the calcite antigorite tie-line in the CaO-MgO-SiO_2 system. This reflects silica enrichment, decarbonation and stable Mg/Si ratio characteristics of hydrothermally altered dolomitic protoliths. The preservation of algal textures and the presence of *Anthracoporella spectabilis* confirms a Late Carboniferous age for the original dolostone, while talc is linked to Permian

hydrothermal activity associated with Gondwana rifting and Panjal magmatism.

4. Trace element analysis reveals moderate chromium concentration (100–300 ppm) and elevated sulfur content (up to 5700 ppm in ST15) likely derived from pyrite and hematite. The potential presence of Cr^{6+} raises environmental considerations, particularly under oxidative weathering. However, the absence of other toxic elements (As, Pb, Cd, Hg) suggests the soapstone has low overall environmental risk and remains suitable for industrial use.

Data availability statement

The original contributions presented in the study are included in the article/supplementary material, further inquiries can be directed to the corresponding authors.

Author contributions

KUM: Conceptualization, Data curation, Formal Analysis, Investigation, Methodology, Software, Validation, Writing – original draft, Writing – review and editing. MSM: Conceptualization, Data curation, Investigation, Resources, Software, Supervision, Validation, Visualization, Writing – original draft, Writing – review and editing. GK: Data curation, Funding acquisition, Investigation, Methodology, Project administration, Validation, Writing – review and editing. SKA: Data curation, Formal Analysis, Investigation, Methodology, Software, Validation, Writing – review and editing. SA: Data curation, Investigation, Software, Validation, Writing – review and editing. HTJ: Data curation, Formal Analysis, Investigation, Methodology, Validation, Writing – review and editing. KS: Data curation, Investigation, Methodology, Software, Validation, Visualization, Writing – review and editing. EB: Data curation, Investigation, Methodology, Validation, Writing – review and editing. AA: Data curation, Investigation, Methodology, Project administration, Validation, Writing – review and editing.

Funding

The author(s) declare that no financial support was received for the research and/or publication of this article.

Acknowledgments

The authors extend their sincere gratitude to the respected reviewers, the Editor-in-Chief, and the Handling Editor. We also extend our gratitude to the Coordinator of the Institute of Geology, for her generous support and facilitation during the fieldwork and all other members of different companies mentioned in methodology for their valuable assistance in sample collection and analysis. Finally, we appreciate the constructive feedback from reviewers, which helped improve the quality of this manuscript.

Conflict of interest

The authors declare that the research was conducted in the absence of any commercial or financial relationships that could be construed as a potential conflict of interest.

Generative AI statement

The author(s) declare that no Generative AI was used in the creation of this manuscript.

Publisher's note

References

Ahsan, N., and Chaudhry, M. N. (1998). *Facies and microfacies analysis of kawagarh formation of Hazara Basin, Pakistan. 13th himalaya-karakoram-tibet workshop*, 31. Abstract, Geological Bulletin, Peshawar University, 5–6.

Anderson, D. L., Mogk, D. W., and Childs, J. F. (1990). Petrogenesis and timing of talc formation in the Ruby Range, southwestern Montana. *Econ. Geol.* 85 (3), 585–600. doi:10.2113/gsecongeo.85.3.585

Barbosa, S. E., and Castillo, L. A. (2023). Morphological and physicochemical properties of macrocrystalline talc from Argentine. *Minerals* 13 (5), 683. doi:10.3390/min13050683

Blount, A. M., and Vassiliou, A. H. (1980). The mineralogy and origin of the talc deposits near Winterboro, Alabama. *Econ. Geol.* 75 (1), 107–116. doi:10.2113/gsecongeo.75.1.107

Bucher, K., Frey, M., Winkler, H. G., and Frey, M. (2002). *Petrogenesis of metamorphic rocks*, 341. Berlin: Springer.

Bucher, K., and Grapes, R. (2011). Metamorphism of pelitic rocks (metapelites). *Petrogenesis Metamorph. Rocks*, 257–313. doi:10.1007/978-3-540-74169-5_7

Calkins, J. A., Offield, T. W., Abdullah, S. K. M., and Ali, S. T. (1975). Geology of the southern Himalaya in Hazara, Pakistan, and adjacent areas.

Carroll, D. (1970). "Trace elements in weathering," in *Rock weathering* (Boston, MA: Springer US), 145–168.

Chaudhry, M. N., and Ghazanfar, M. (1990). Position of the main central thrust in the tectonic framework of western himalaya. *Tectonophysics* 174 (3-4), 321–329. doi:10.1016/0040-1951(90)90329-7

Chaudhry, M. N., Kasuri, R. A., and Ahsan, N. (1997). Facies, microfacies, diagenesis and environment of deposition of lumshiwal formation at thub top near ayubia, district Abbottabad. *Pak. J. Hydrocarbon Res.* 9, 57–66.

Cuitino, L. (2010). Mineralogía y génesis del yacimiento de lapislazuli, Flor de los andes, Coquimbo, Norte de Chile. *Andean Geol.* (27).

Dejan, M., Ramesh, C., Gupta, Z. Y., Zaja-Milatovic, S., and Aschner, M. (2011). Chapter 34 – manganese. 439–450. doi:10.1016/B978-0-12-382032-7.10034-7

Easthouse, G., Hoover, W., Teng, F.-Z., Condit, C., Pike, C., Wang, Z.-Z., et al. (2025). Formation of talc in the subduction interface: Mg isotopes demonstrate Mg loss over Si gain. *Geology* 53, 398–403. doi:10.1130/G52538.1

Evans, B. W., and Guggenheim, S. (1988). Talc, pyrophyllite, and related minerals. *Rev. Mineralogy Geochem.* 19 (1), 225–294.

Fazal, A. G., Umar, M., Shah, F., Miraj, M. A. F., Janjuhah, H. T., Kontakiotis, G., et al. (2022). Geochemical analysis of cretaceous shales from the Hazara Basin, Pakistan: provenance signatures and paleo-weathering conditions. *J. Mar. Sci. Eng.* 10, 800. doi:10.3390/jmse10060800

Ghazanfar, M., Chaudary, M. N., Pervaiz, K., Qayyum, M., and Ahmed, R. (1990). Geology and structure of kuza-dunga gali-ayubia area, hazara-potwar Basin with a reference to hydrocarbon prospects of attock-hazara fold and thrust belt, Pakistan. *J. Hydrocarbon Res.* 2 (2), 43–55.

Groppo, C. T., and Compagnoni, R. (2007). Metamorphic veins from the serpentinites of the Piemonte Zone, western Alps, Italy: a review. *Period. Mineral.* 76, 127–153.

Groves, J. R., and Yue, W. (2009). Foraminiferal diversification during the late Paleozoic ice age. *Paleobiology* 35 (3), 367–392. doi:10.1666/0094-8373-35.3.367

Hecht, L., Freiberger, R., Gilg, H. A., Grundmann, G., and Kostitsyn, Y. A. (1999). Rare earth element and isotope (C, O, Sr) characteristics of hydrothermal carbonates: genetic implications for dolomite-hosted talc mineralization at Göpfersgrün (Fichtelgebirge, Germany). *Chem. Geol.* 155 (1-2), 115–130. doi:10.1016/s0009-2541(98)00144-2

Hill, G. (2018). *Fluid inclusion and stable isotope investigation of hydrothermal talc and chlorite deposits in southwest Montana*. Master's thesis, Montana Tech of The University of Montana.

Joshi, P., and Sharma, R. (2015). Fluid inclusion and geochemical signatures of the talc deposits in Kanda area, Kumaun, India: implications for genesis of carbonate hosted talc deposits in Lesser Himalaya. *Carbonates Evaporites* 30 (2), 153–166. doi:10.1007/S13146-014-0196-3

Kazmi, A. H., and Jan, M. Q. (1997). *Geology and tectonics of Pakistan* (Karachi: Graphic Publishers).

Konhauser, K. O., Lalonde, S. V., Planavsky, N. J., Pecoits, E., Lyons, T. W., Mojzsis, S. J., et al. (2011). Aerobic bacterial pyrite oxidation and acid rock drainage during the Great Oxidation Event. *Nature* 478 (7369), 369–373. doi:10.1038/NATURE10511

Latif, M. A. (1970). Explanatory notes on the Geology of southeastern Hazara, to accompany the revised geological map. *Wien Jb. Geol. BA, Sonderb* 15.

Le Fort, P. (1975). Himalayas: the collided range – present knowledge of the continental arc. *Am. J. Sci.* 275-A, 1–44.

McGrath, M. (2017). *Constraints on the petrogenesis of a proterozoic talc deposit in southwestern Montana: a petrological and geochemical study doctoral dissertation*. University of Pittsburgh.

Moine, B., Fortune, J. P., Moreau, P., and Viguier, F. (1989). Comparative mineralogy, geochemistry, and conditions of formation of two metasomatic talc and chlorite deposits; Trimouns (Pyrenees, France) and Rabenwald (Eastern Alps, Austria). *Econ. Geol.* 84 (5), 1398–1416. doi:10.2113/gsecongeo.84.5.1398

Molnar, P., and Tapponnier, P. (1975). Cenozoic Tectonics of Asia: effects of a Continental Collision: features of recent continental tectonics in Asia can be interpreted as results of the India-Eurasia collision. *Science* 189 (4201), 419–426. doi:10.1126/science.189.4201.419

Ogasawara, M., Fukuyama, M., Siddiqui, R. H., and Zhao, Y. (2019). Origin of the Ordovician Mansehra granite in the NW Himalaya, Pakistan: constraints from Sr–Nd isotopic data, zircon U–Pb age and Hf isotopes. *Geol. Soc. Lond. Spec. Publ.* 481 (1), 277–298. doi:10.1144/sp481.5

O'Hanley, D. S. (1996). *Serpentinites: records of tectonic and petrological history*. New York, NY: Oxford University Press, 277.

Petterson, M. G., and Windley, B. F. (1985). RbSr dating of the Kohistan arc-batholith in the Trans-Himalaya of north Pakistan, and tectonic implications Himalaya of north Pakistan, and tectonic implications. *Earth Planet. Sci. Lett.*, 74(1), 45–57. doi:10.1016/0012-821x(85)90165-7

Prochaska, W. (1989). Geochemistry and genesis of Austrian talc deposits. *Appl. Geochem.* 4 (5), 511–525. doi:10.1016/0883-2927(89)90008-5

Pudsey, C. J., Coward, M. P., Luff, I. W., Shackleton, R. M., Windley, B. F., and Jan, M. Q. (1985). Collision zone between the Kohistan arc and the Asian plate in NW Pakistan. *Earth Environ. Sci. Trans. R. Soc. Edinb.* 76 (4), 463–479. doi:10.1017/s026359330001066x

Rehman, S. U., Munawar, M. J., Shah, M. M., Ahsan, N., Kashif, M., Janjuhah, H. T., et al. (2023). Diagenetic evolution of upper cretaceous kawagarh carbonates from attock Hazara fold and thrust belt, Pakistan. *Minerals* 13 (11), 1438. doi:10.3390/min13111438

Riding, R. (2000). Microbial carbonates: the geological record of calcified bacterial–algal mats and biofilms. *Sedimentology* 47, 179–214. doi:10.1046/j.1365-3091.2000.00003.x

Rowland, S. M., and Shapiro, R. S. (2002). Reef patterns and environmental influences in the Cambrian and earliest Ordovician, 95, 128. doi:10.2110/pec.02.72.0095

Sajid, M., Andersen, J., and Arif, M. (2018). Petrogenesis and tectonic association of rift-related basic Panjal dykes from the northern Indian plate, North-Western Pakistan: evidence of high-Ti basalts analogous to dykes from Tibet. *Mineralogy Petrology* 112, 415–434. doi:10.1007/s00710-017-0536-9

Scambelluri, M., Bebout, G. E., Belmonte, D., Gilio, M., Campomenosi, N., Collins, N., et al. (2016). Carbonation of subduction-zone serpentinite (high-pressure ophicarbonate; Ligurian Western Alps) and implications for the deep carbon cycling. *Earth Planet. Sci. Lett.* 441, 155–166. doi:10.1016/j.epsl.2016.02.034

Schandl, E. S., Gorton, M. P., and Sharara, N. A. (2002). The origin of major talc deposits in the Eastern Desert of Egypt: relict fragments of a metamorphosed carbonate horizon? *J. Afr. Earth Sci.* 34 (3-4), 259–273. doi:10.1016/s0899-5362(02)00024-6

Shin, D., and Lee, I. (2003). Carbonate-hosted talc deposits in the contact aureole of an igneous intrusion (Hwanggangri mineralized zone, South Korea): geochemistry, phase relationships, and stable isotope studies. *Ore Geol. Rev.* 22 (1-2), 17–39. doi:10.1016/s0169-1368(02)00085-9

Treloar, P. J., Rex, D. C., Guise, P. G., Coward, M. P., Searle, M. P., Windley, B. F., et al. (1989). K-Ar and Ar-Ar geochronology of the Himalayan collision in NW Pakistan: constraints on the timing of suturing, deformation, metamorphism and uplift. *Tectonics* 8 (4), 881–909. doi:10.1029/tc008i004p00881

Vezzoni, S., Pieruccioni, D., Galanti, Y., Biagioni, C., and Dini, A. (2020). Permian hydrothermal alteration preserved in polymetamorphic basement and constraints for ore-genesis (Alpi Apuane, Italy). *Geosciences* 10 (10), 399. doi:10.3390/geosciences10100399

Woelfler, A., Prochaska, W., and Fritz, H. (2015). Shear zone related talc mineralization's in the Veitsch Nappe of the eastern greywacke zone (Eastern Alps, Austria). *Austrian J. Earth Sci.* 108 (1), 50–72. doi:10.17738/ajes.2015.0004

Zaheer, M., Khan, M. R., Mughal, M. S., Janjuhah, H. T., Makri, P., and Kontakiotis, G. (2022). Petrography and lithofacies of the siwalik group in the core of hazara-kashmir syntaxis: implications for middle stage himalayan orogeny and paleoclimatic conditions. *Minerals* 12 (8), 1055. doi:10.3390/min12081055

Zedef, V., Russell, M. J., Fallick, A. E., and Hall, A. J. (2000). Genesis of vein stockwork and sedimentary magnesite and hydromagnesite deposits in the ultramafic terranes of southwestern Turkey: a stable isotope study. *Econ. Geol.* 95 (2), 429–445. doi:10.2113/95.2.429